https://doi.org/10.5194/cp-2023-82
Preprint. Discussion started: 17 October 2023

Climate of the Past Discussions

Multiple thermal AMOC thresholds in the intermediate complexity model Bern3D

Markus Adloff[1,2*], Frerk Pöppelmeier[1,2], Aurich Jeltsch-Thömmes[1,2], Thomas F. Stocker[1,2], Fortunat Joos[1,2]

[1] Centre for Environmental Physics, University of Bern, Switzerland
[2] Oeschger Centre for Climate Change Research, University of Bern, Switzerland

*Contact: markus.adloff@unibe.ch

Abstract

Variations of the Atlantic Meridional Overturning Circulation (AMOC) are associated with Northern Hemispheric and global climate shifts. Thermal thresholds of the AMOC have been found in a hierarchy of numerical circulation models, and there is an increasing body of evidence for the existence of highly sensitive AMOC modes where small perturbations can cause disproportionately large circulation and hence climatic changes. We discovered such thresholds in simulations with the intermediate complexity Earth system model Bern3D, which is highly computationally efficient allowing for studying this non-linear behaviour systematically over entire glacial cycles. By simulating the AMOC under different magnitudes of orbitally-paced changes in radiative forcing over the last 800,000 years, we show that up to three thermal thresholds are crossed during glacial cycles in Bern3D, and that thermal forcing could have destabilised the AMOC repeatedly. We present the circulation and sea ice patterns that characterise the stable circulation states between which the model oscillates during a glacial cycle, and assess how often and when thermal forcing could have preconditioned the AMOC for abrupt shifts over the last 800 kyr.

1. Introduction

The Atlantic Meridional Overturning Circulation (AMOC) transports warm waters from the Southern Hemisphere and the Mexican Gulf towards the Nordic Seas, until the vertical density gradient becomes unstable and the now cool and salty water subducts and forms North Atlantic Deep Water (NADW). This water mass moves southwards along the western boundary of the Atlantic boundary until it encounters the denser Antarctic Bottom Water (AABW) and slowly rises and upwells in the Southern Ocean, being ultimately incorporated again either into AABW or the lighter Antarctic Intermediate Water (AAIW). The northward heat transport of the AMOC shapes regional and global climate by pushing the polar front north by several degrees of latitude, producing a milder climate in Europe and Greenland than predicted from latitude/insolation alone (Ruddiman and McIntyre 1981, Bard et al. 1987), moving the Intertropical Convergence Zone (ITCZ) and monsoon systems (Wang et al., 2001, Bozbiyik et al, 2011), and interacting with North Pacific Deep Water Formation and climate (Okazaki et al., 2010, Menviel et al., 2012, Praetorius and Mix, 2014). The AMOC furthermore shapes biological productivity by regulating nutrient supply to the surface. It influences deep ocean nutrient and oxygen concentrations by accumulating respired carbon on its southward path in the Atlantic (Broecker, 1991), and by affecting the ventilation of the Pacific thermocline (Tetard et al., 2017, Joos et al., 2017), and by modulating atmospheric greenhouse gas concentrations (e.g., Fischer et al., 2018). Rapid changes in AMOC and hence Atlantic heat redistribution occurred repeatedly during the last glacial, termed Heinrich

https://doi.org/10.5194/cp-2023-82
Preprint. Discussion started: 17 October 2023

(Heinrich, 1988, Broecker, 1994) and Dansgaard-Oeschger events (Dansgaard et al., 1993), and had regional and global impacts on ecosystems and humans (e.g. Severinghaus et al., 2009, Timmermann and Friedrich, 2016). Yet,the factors determining AMOC stability in the past and future are not fully understood.

As part of the thermo-haline circulation, the AMOC is sensitive to both salinity and thermal forcing. Depending on the location of deep water formation in both hemispheres, the AMOC can switch between stable circulation states - either gradually or abruptly - as local vertical density gradients, sea ice extent, and meridional heat and salinity gradients change: Numerical experiments showed that large freshwater inputs into the North Atlantic can theoretically cause abrupt shifts from a vigorous circulation state to a temporarily subdued circulation (e.g. Stocker and Wright, 1991, reviews by Weijer et al., 2019, Jackson et al., 2023). Such possible circulation state shifts were first identified in box models (Stommel 1961) and confirmed in intermediate complexity models and global circulation models (Jackson and Wood, 2018, review in Jackson et al, 2023). This mechanism could explain reconstructed sudden AMOC state shifts in the Pleistocene, likely caused by large freshwater fluxes from melting continental ice shields and increased iceberg transport into the North Atlantic at the onset of Heinrich Events (Broecker, 1994, Grousset et al., 2000). It has also been found that the melting Greenland ice sheet could weaken the AMOC in the future, if the meltwater gets transported into the convection zones of the Labrador Sea (Swingedouw et al., 2022).

Besides Heinrich Event-like AMOC shifts from more to less vigorous circulation in response to strong freshwater forcing, there is increasing evidence for metastable AMOC states in-between the glacial and interglacial circulation end-members. In some numerical models, and for narrow parameter ranges (e.g. atmospheric CO_2 concentrations, ice sheet configurations), the AMOC in such intermediate climate states is sensitive to small internal or external variability and can sustain spontaneous oscillations (e.g. Brown and Galbraith, 2016, Vettoretti et al., 2022, review of CMIP6 models in Malmierca-Vallet et al., 2023). Some of these oscillations could be analogs to Dansgaard-Oeschger events that have been identified during intermediate glacial climate conditions specifically during Marine Isotope Stage (MIS) 3, and are thought to be caused by internal feedbacks that amplify small changes of the North Atlantic salinity balance (Armstrong et al., 2022). Meteoric and terrestrial freshwater supplies to the surface ocean are climate sensitive, as is the salt rejection associated with sea ice formation, and are thus both impacted by and impacting AMOC. Feedbacks similarly exist for the salinity transport from the tropics to the North Atlantic, global circulation patterns and the salinity gradients which determine salt transport into the Atlantic basin through the Bering Strait, Drake Passage and from the Indian Ocean (e.g. Rahmstorf 1996). Besides salinity changes, numerical experiments also show that vertical temperature distribution affects AMOC stability (Haskins et al., 2020). Thermal forcing of the North Atlantic has been found to cause gradual changes in AMOC strength, while thermal forcings applied to the Southern Ocean can cause abrupt AMOC state changes similar to freshwater forcings in the North Atlantic (Oka et al., 2021).

So far simulations of thermal AMOC thresholds have been done with computationally expensive numerical models, and the implications of the existence of AMOC instability and thermal thresholds have not been tested across entire glacial cycles. While providing crucial

https://doi.org/10.5194/cp-2023-82
Preprint. Discussion started: 17 October 2023


Climate of the Past Discussions

process understanding, direct comparisons of these simulations to proxy records are therefore challenging.

Here, we demonstrate the existence of hysteresis and mode shifts in the AMOC in the intermediate complexity model Bern3D, in the absence of freshwater hosing. Instead, we only apply changes in the radiative forcing to the atmosphere-ocean system. We provide a comprehensive description of the underlying processes and elucidate the influence of radiative changes on the AMOC dynamics in the Bern3D model during orbitally-forced glacial-interglacial cycles.

2. Methods

We employed the Bern3D intermediate complexity model version 2.0 to investigate the AMOC behaviour under a wide range of radiative forcing. The Bern3D model comprises a 3D ocean component with a 40x41 horizontal grid and 32 depth layers, along with a 2D atmosphere (spatially-explicit energy-moisture balance with prescribed wind fields) and dynamic sea-ice. The model explicitly calculates the thermo-haline circulation with a frictional-geostrophic flow (Edwards et al., 1998) and contains parameterizations to account for isopycnal diffusion and eddy-turbulence via the Gent-McWilliams parameterization (Griffies, 1998). Temperature and salinity are dynamically transported by the physical ocean model and respond to static wind fields and changing atmospheric 2D energy and moisture balance, sea ice formation and external forcings. Bern3D explicitly calculates Pacific-Atlantic transport through the Bering Strait, and freshwater flux corrections are only imposed in the Weddell Sea, and compensated for in the Southern Ocean to induce stronger deep water formation.

Table 1: Overview of the model experiments in this study. In set A, radiative forcing from dust is scaled linearly with $\delta^{18}O$ and assuming different magnitudes at LGM as given in parentheses.

https://doi.org/10.5194/cp-2023-82
Preprint. Discussion started: 17 October 2023

Climate of the Past Discussions
Open Access
EGU

Simulation Set	Simulation ID	Starting point and length	Forcing	Purpose
A	A0	MIS 19 spin-up 787500 years	orbital+GHG+dust(0 W/m^2)	test AMOC changes in response to transient glacial-interglacial radiative forcing
	A1		orbital+GHG+dust(-1 W/m^2)	
	A2		orbital+GHG+dust(-2 W/m^2)	
	A3		orbital+GHG+dust(-3 W/m^2)	
	A4		orbital+GHG+dust(-4 W/m^2)	
	A5		orbital+GHG+dust(-5 W/m^2)	
	A6		orbital+GHG+dust(-6 W/m^2)	
	A7		orbital+GHG+dust(-7 W/m^2)	
	A8		orbital+GHG+dust(-8 W/m^2)	
B	B.slow	PI spin-up, 105 kyr	linear change in RF from 0 to -10 W/m^2 over 50 kyr and recovery over next 50 kyr	identify processes that cause AMOC shifts under radiative forcing
	B.slow.a	year 23000 of B.slow, 20 kyr	0.1 Sv freshwater input over 100 yr	test AMOC stability at different time steps in B.slow
	B.slow.b	year 24500 of B.slow, 20 kyr		
	B.slow.c	year 28500 of B.slow, 5 kyr		
	B.slow.d	year 47000 of B.slow, 5 kyr		
	B.fast.PI	PI spin-up, 25 kyr	linear change in RF from 0 to -10 W/m^2 over 10 kyr and recovery over next 10 kyr with different orbital parameters	test dependence of AMOC response to radiative forcing to orbital constellation
	B.fast.21ka	PI spin-up, 25 kyr		
	B.fast.30ka	PI spin-up, 25 kyr		
	B.fast.50ka	PI spin-up, 25 kyr		
	B.fast.80ka	PI spin-up with, 25 kyr		

We conducted two sets of simulations with the Bern3D model (Table 1). In set A, comprising nine simulations, we fully transiently simulated the last 800 kyr by imposing changes in orbital configuration, albedo changes from prescribed variation in ice sheet extent, and global average radiative forcing from the well-mixed greenhouse gases (GHG) CO_2 and CH_4 (combined here labelled as the 'standard forcing'). The runs started from an interglacial steady state (50 kyr with pre-industrial (PI) conditions and 2 kyr of re-adjustment to the radiative balance of MIS 19c). Orbital (Berger, 1978, Berger and Loutre, 1991), GHG (Bereiter et al., 2015, Loulergue et al., 2008, Joos and Spahni, 2008), and ice sheet albedo forcing (i.e. the standard forcing) is identical in each run (Fig. 1). Ice sheet extent is following the benthic $\delta^{18}O$ LR04 stack (Lisiecki & Raymo, 2005) smoothed by averaging over a 10000-year moving window for the rest of the past 800 kyr. Radiative forcing from atmospheric optical depth changes due to changes in aerosols and dust, termed dust forcing, varies between the simulations. The maximum LGM radiative dust forcing is a free parameter, ranging from 0 to -8 W/m^2 relative to PI (Simulations A.0 to A.8), and is scaled linearly with the smoothed LR04 stack to achieve a forcing time series. The range of the resulting combined radiative forcing is between -3 and -10 W/m$^{2.}$ This range brackets estimates of maximum reductions in global mean radiative forcing at the LGM of 7 - 8 W/m^2 due to albedo, greenhouse gas, and aerosol effects (Albani et al., 2018). The imposed forcings resulted in global mean surface temperature (GMST) differences between the LGM and PI of -3 to -9.6°C. This temperature range encompasses most of the LGM-PI range reported in studies investigating the Paleo Model Intercomparison Project (PMIP) 2, PMIP3, and PMIP4, which range from -3.1 to -7.2°C (Masson-Delmotte et al., 2013, Kageyama et al., 2021). Furthermore, these simulations are also consistent with proxy-based reconstructions that indicate GMST differences between -2 and -8°C (Tierney et al., 2020), as well as covering the -6.1°C GMST difference as constrained by a recent data assimilation study with the

https://doi.org/10.5194/cp-2023-82
Preprint. Discussion started: 17 October 2023

Climate of the Past Discussions

CESM model (Tierney et al., 2020). Freshwater fluxes associated with the build-up and disintegration of continental ice sheets and glaciers are not taken into account in any of the simulations presented here. We also keep the topography constant and do not close the Bering Street.

Simulation set B was designed to investigate the mechanisms behind radiation-driven AMOC changes under more idealised boundary conditions. This simulation set includes one long run with "slowly" changing radiative forcing (105 kyr, B.slow), five short simulations with "fast" changing forcing (25 kyr, B.fast), and four simulations branched off from B.slow at different points in time. B.slow started from a pre-industrial state, followed by a linearly decreasing negative radiative forcing over 50 kyr, followed by a linear increase of forcing back to the initial state also over 50 kyr (Figure 4). We continued the simulation for an additional 5 kyr under constant, pre-industrial conditions to let the model re-equilibrate. Setup of B.fast.PI is analogous to B.slow with the radiation decrease and consecutive increase spanning 20 kyrs. The simulations started from a steady state with pre-industrial orbital and GHG configuration, and were run with orbital configurations of PI, 21, 30, 50 and 80 kyrBP (simulations B.fast.PI, B.fast.21ka, B.fast.30ka, B.fast.50ka, B.fast.80ka, respectively).

At four specific time points in B.slow, we branched off simulations to test the AMOC stability by keeping all forcings constant, but at the same time applying a small freshwater hosing to the North Atlantic (45°N-70°N) with a magnitude of 0.1 Sv over 100 years. If the AMOC is in a stable state it should recover from these freshwater perturbations returning to its initial strength, while an unstable AMOC should transition into a new circulation mode.

We incorporated three passive circulation tracers ('dyes') in set B. Each of these dye tracers is restored to 1 at the surface of a chosen region (Fig. SI.1), and to zero elsewhere in the surface ocean, and has no sources or sinks below the surface. In the deep ocean, the dye tracer concentration is hence diluted only by mixing with other water masses sourced from other regions. These artificial dye tracers allow us to track the dispersal of North Atlantic Deep Water (NADW), Antarctic Intermediate Water (AAIW) and Antarctic Bottom Water (AABW) in the ocean interior.

3. Results and Discussion

We first investigate the response of the AMOC to changes in orbital configuration and radiative forcing as transiently simulated in our 800 kyr-long simulations of set A. We aim to provide a comprehensive understanding of radiation-driven AMOC dynamics on glacial-interglacial timescales. Subsequently, we utilise the more idealised setup of simulation set B to further examine the underlying mechanisms driving these changes in more detail.

3.1. AMOC changes over the past eight glacial cycles

https://doi.org/10.5194/cp-2023-82
Preprint. Discussion started: 17 October 2023

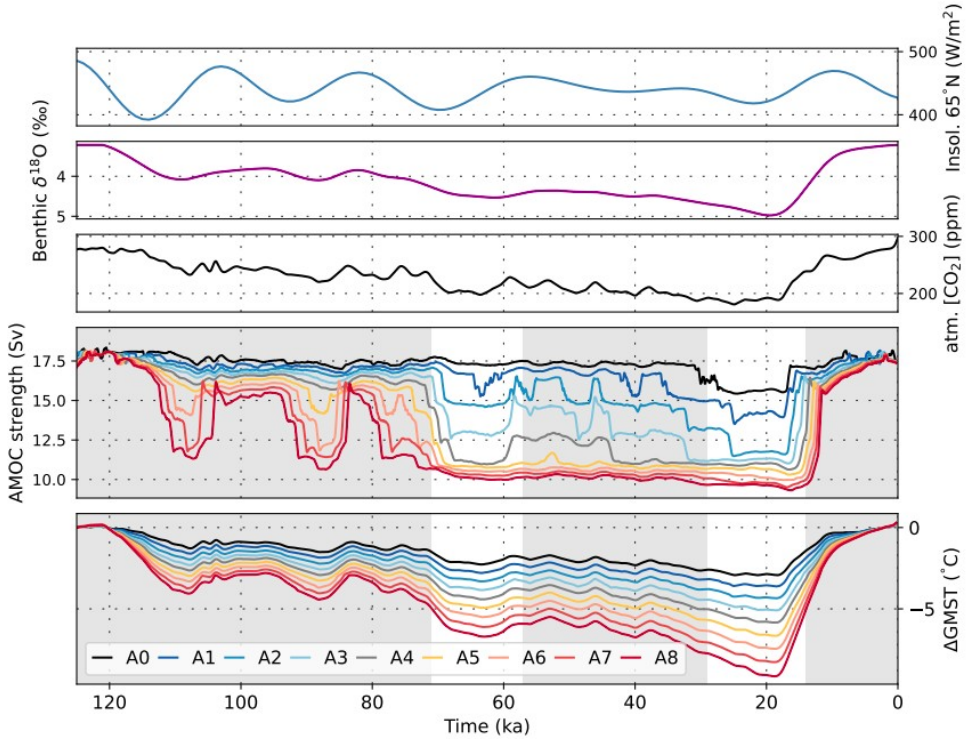

Figure 1: Forcings, AMOC and temperature response over the last 125 kyr of simulation ensemble A. The upper three panels show July Insolation at 65°N, benthic $\delta^{18}O$ (10 kyr spline of LR04, Lisiecki and Raymo, 2005) used to scale the dust forcing and reconstructed atmospheric CO_2 (Bereiter et al., 2015), smoothed with a second-order lowpass filter (cutoff frequency: 1/2000). The lower two panels show the 500 yr running mean of simulated AMOC strength and GMST deviations from the PI in every simulation of simulation set A. Colours in the lower two panels differentiate between simulations with different amplitudes of the radiative forcing (see Methods).

In our simulations, radiative forcing- and orbitally-driven temperature changes result in both gradual and abrupt AMOC shifts during each of the last eight glacial cycles. Fig. 1 illustrates the simulated AMOC threshold behaviour during these changes over the entire last glacial cycle (past 125 kyr) with the different dust forcing scalings. Abrupt changes in AMOC strength are present in every simulation, with larger changes occurring under stronger forcing. The magnitude of the dust forcing also determines the phase of the glacial cycle during which the AMOC is most sensitive to radiative forcing: pronounced reductions in radiative forcing under strong scaling result in a shift to the weakest AMOC state early in the last glacial cycle, which is then insensitive to further changes induced by additional reductions in radiative forcing later on. Conversely, under weaker scaling, the initial decrease in forcing is insufficient to shift the AMOC out of its interglacial circulation mode.

https://doi.org/10.5194/cp-2023-82
Preprint. Discussion started: 17 October 2023

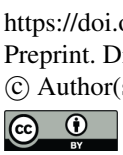

Climate of the Past Discussions
Open Access
EGU

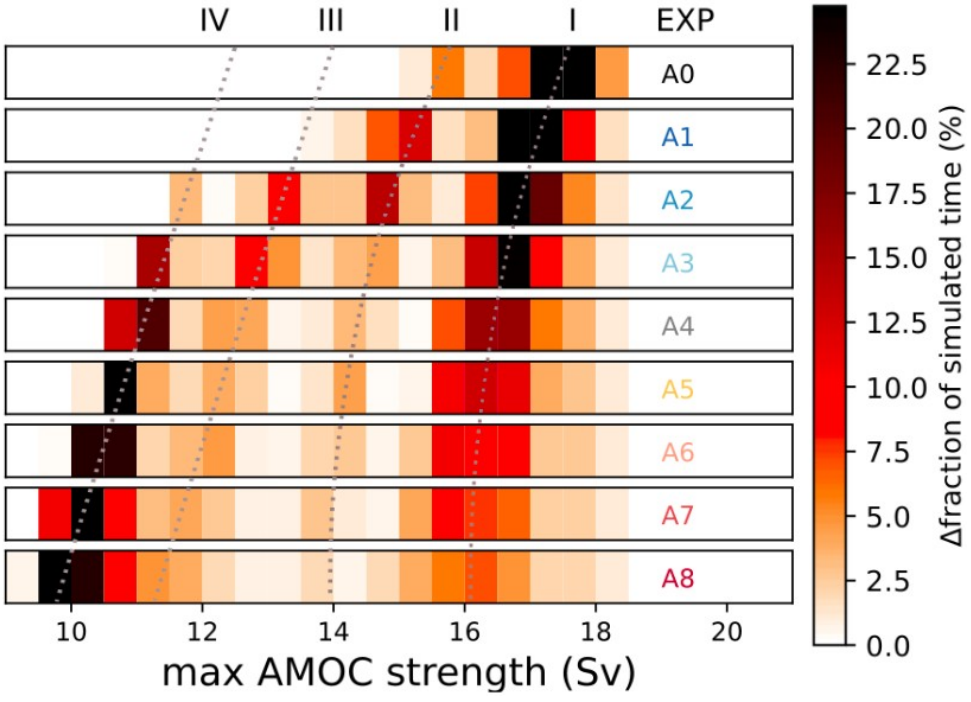

Figure 2: Fraction of each simulation in simulation set A (each over 800 kyr) during which a given maximum AMOC strength was simulated. Each row shows the results of one simulation, with the simulation ID on the right end of the column in colours that correspond to the lines in Fig 1. The bins are 0.5 Sv wide and four relative maxima in occurrence, exhibiting distinct AMOC states, I – IV, are indicated by dotted lines.

All simulations reveal multiple intermediate stable states between the glacial and interglacial end-members. These states manifest as distinct bands of increased occurrence in Fig 2, which displays the fraction of the entire simulated period of 800 kyr during which the AMOC exhibits a given strength (binned into 0.5 Sv intervals). In total, we identified up to four stable circulation modes in simulation set A, between which the AMOC transitions (Fig 2), although the weakest stable state is never reached in the simulations with the smallest radiative forcing (i.e., the simulations with the warmest climate throughout the glacial). The simulations A3 and A4 with intermediate glacial-interglacial temperature changes (LGM-PI ΔGMST -5 to -6 °C, similar to the -6.1 °C constrained by Tierney et al., 2020) exhibit AMOC evolutions that predominantly transition between the interglacial (state I, ~16-17 Sv) and glacial stable state (state IV, ~11 Sv), with two rarer intermediate circulation modes in-between. Further, Figure 2 highlights that the magnitude of the applied dust forcing scaling has a marginal effect on the absolute AMOC strength in each stable circulation mode. Additional reductions in radiative forcing after the AMOC already transitioned to the stable glacial circulation mode only causes minor additional AMOC weakening, without going through another abrupt transition. AMOC strengths that occur most often during the simulated 800 kyr are also the most stable ones. In particular, the glacial and interglacial 'end-member' circulation states I and IV are the most stable with the highest occurrences:

https://doi.org/10.5194/cp-2023-82
Preprint. Discussion started: 17 October 2023

Climate of the Past Discussions
Open Access
EGU

The AMOC is in either of these two states for 62-85% of the simulated 800 kyr in all simulations. The exact number of and partitioning between glacial and interglacial states depend on the dust forcing scaling. The AMOC is found in the intermediate circulation states II and III most commonly under weak dust forcing. Instead, for stronger forcings, these states are increasingly skipped. Thus, it appears that there is a tendency towards bi-modal AMOC stability under strong forcing scaling, where the AMOC is only either in the glacial or interglacial circulation state.

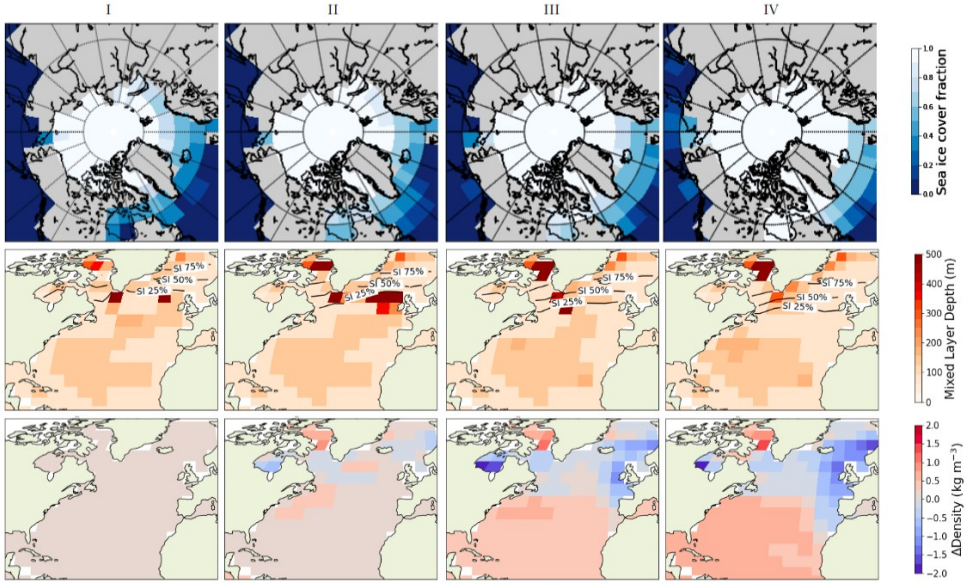

Figure 3: North Atlantic sea ice extent, annually-averaged mixed layer depth and differences in surface water density from the interglacial circulation state (state I) in the four circulation states identified in Fig 2 for simulation A3. Here we defined the mixed layer depth as the most shallow depth at which the density is >= 0.5 kg/m^3 different from the surface density. Contour lines indicate annually averaged sea ice coverage.

The interglacial circulation state (state I in Figs. 2 and 3) is characterised by NADW formation in the subpolar North Atlantic, specifically south of Greenland and close to the British Isles, as indicated by the annually-averaged mixed layer depth. At the first stable intermediate AMOC state (II), deep water formation is enhanced in the Eastern Atlantic while it weakens in the West as sea ice expands further South (Fig. 3). The next intermediate-stable circulation state (III) is marked by a reduction in deep water formation in the eastern North Atlantic because of local water column stratification. Weakened deep water formation continues south of the sea ice edge in the West. As the northwards transport of subtropical water weakens under further cooling, the AMOC transitions into the glacial stable state (IV). During this state, convection in the North Atlantic is strongly reduced and south-flowing fresh Arctic waters further stratify the water column off the European coast. At this point, additional negative radiative forcing enhances the amplitude of the temperature and salinity anomalies but without further altering the North Atlantic circulation pattern.

https://doi.org/10.5194/cp-2023-82
Preprint. Discussion started: 17 October 2023

Our simulations cover four glacial cycles before the Mid-Brunhes transition (MBT) between MIS 12 and MIS 11 (~430 ka) and four thereafter. This transition is marked by a shift to warmer interglacials with higher atmospheric CO_2 concentrations. There are small differences between the distribution of AMOC states between the two time windows (fig SI.2). In simulations A0 and A1 with no or weak dust forcing, the differences are largest for the strong, interglacial AMOC states. In simulations A2 and A3 with medium dust forcing, differences in the forcing variability during glacial phases before and after the MBT are most relevant, and in simulations with strong dust forcing the minimum AMOC strength during glacials is most different. None of these differences are statistically significant in the two-sided Kolmogrov-Smirnov test even at the 50% confidence level.

3.2. Processes responsible for the AMOC changes

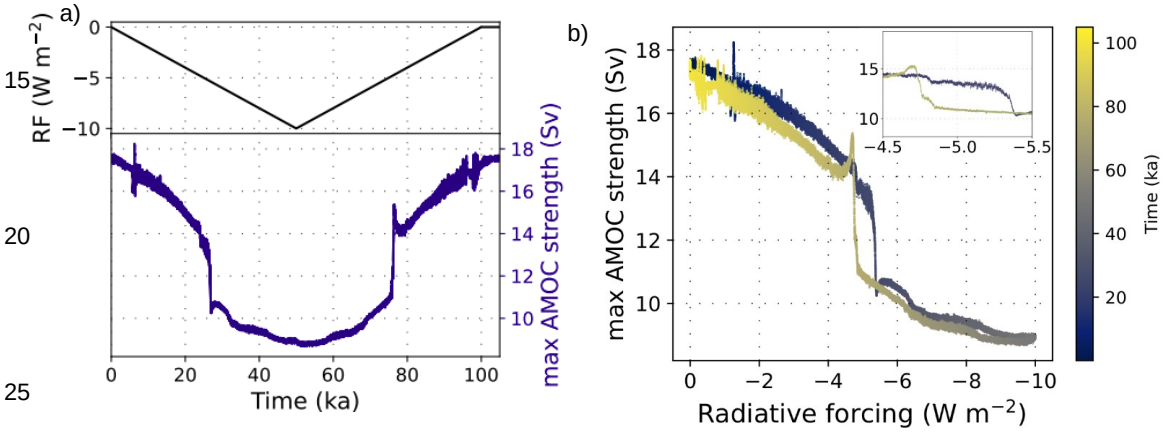

Figure 4: Simulation B.slow: (a) Response of the AMOC to changes in radiative forcing relative to the pre-industrial. The radiative forcing was linearly decreased over 50 kyr to a minimum of -10 W/m2 and then increased again at the same rate. (b) The associated hysteresis loop of the AMOC under the radiative forcing.

https://doi.org/10.5194/cp-2023-82
Preprint. Discussion started: 17 October 2023

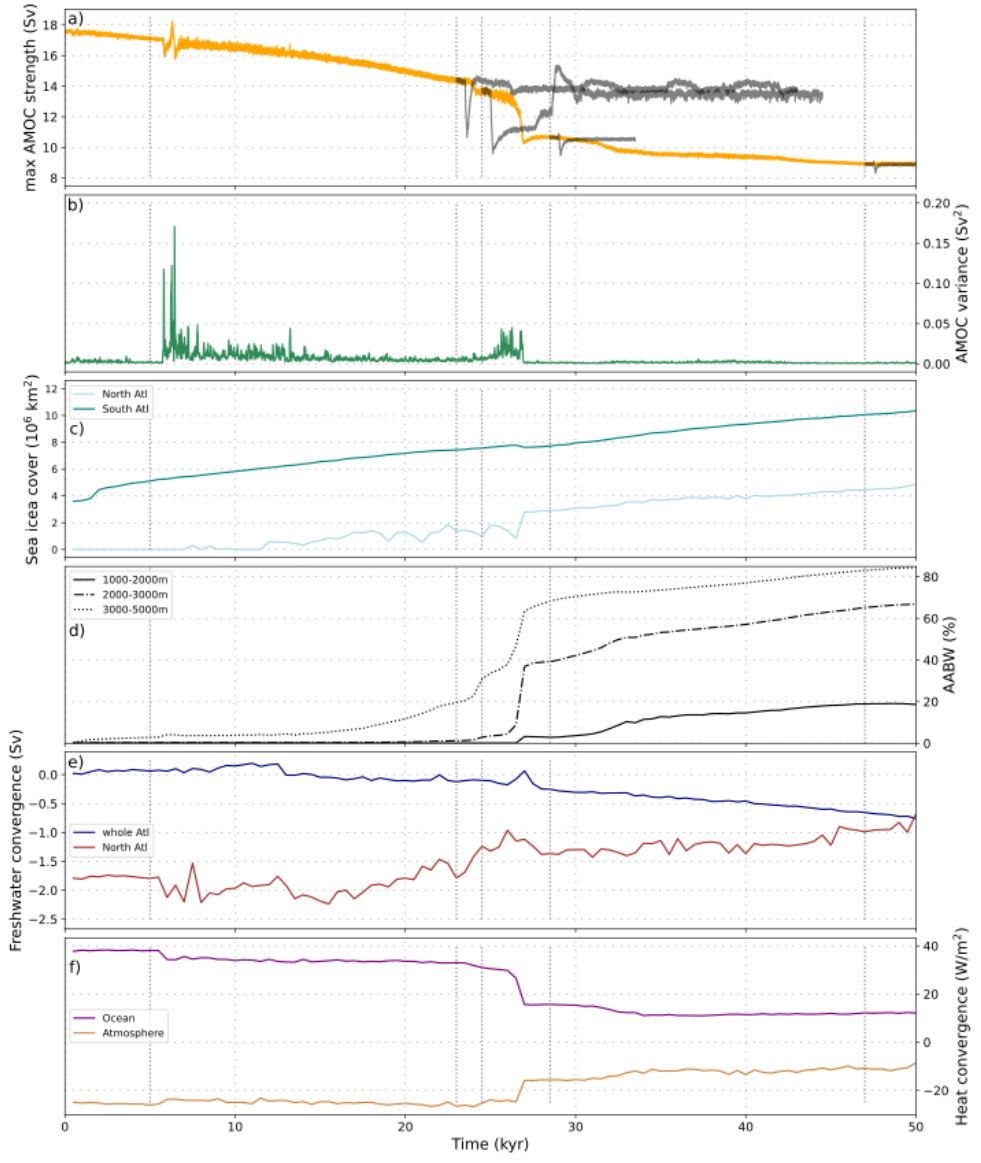

Figure 5: Circulation changes during the cooling phase in simulation B.slow. a) AMOC strength. At four points in time throughout B.slow, simulations were branched off to test the stability of the respective circulation state (shown in dark grey). In these simulations, we kept the radiative forcing constant but applied a small freshwater perturbation after 500 yrs, before allowing the model to re-equilibrate (see Methods). b) AMOC variance. c) Sea ice cover in the Atlantic between 50-60°N ('North Atl') and 50-60°S ('South Atl'). d) percentage of AABW at three different depths in the subpolar North Atlantic (50-60°N). e) Freshwater flux equivalent of marine salt water transport (considering oceanic salinity transport through the southern and northern ocean basin edges following Liu et al., 2017) over the whole Atlantic (35°S-70°N) and the North Atlantic (40°N-70°N). f) Column-integrated heat flux

https://doi.org/10.5194/cp-2023-82
Preprint. Discussion started: 17 October 2023

convergence due to ocean circulation and heat loss to the atmosphere (negative = heat loss by ocean) for the North Atlantic (40°N-70°N). Dotted vertical grey lines indicate time points in the simulation at which we branched off stability tests, and at which we analysed water mass distributions in Fig. 6.

The primary processes controlling the AMOC strength under radiative forcing are density changes due to heat and salinity redistributions. We investigate this in more detail in experiment B.slow (Fig. 4 and 5). As shown in Fig. 4, this experiment is characterised by a slow linear decrease in radiative forcing over 50 kyr, before it is returned to the pre-industrial value over the same time period. Fig. 5 shows how the AMOC, salinity, marine heat transport and sea ice in the North Atlantic change in response to the gradual reduction in radiative forcing. The modelled abrupt transitions to weaker AMOC circulation states are mainly caused by density changes in the North Atlantic, and effectively exert a weak freshwater 'hosing' (i.e. shift to a more positive freshwater balance) in the North Atlantic (Fig. 5e). Initially, heat and salt transport into the North Atlantic and North Atlantic sea ice show little change. Cooling of the Southern Ocean, instead, enhances Southern deep water formation and leads to the expansion of sea ice in the Southern Hemisphere. The resulting strengthening and cooling of AABW spreads an abyssal cold anomaly north into the Atlantic basin. This slowly stabilises the vertical density profile in the North Atlantic from below. Therefore, the response to the reduced radiative forcing involves two processes that operate on very different time scales.

After about 6 kyr, the AMOC starts to weaken as heat advection into the North Atlantic is reduced and sea ice expansion starts in the North Atlantic. The weakened AMOC reduces heat advection and, together with decreasing subtropical evaporation, salt transport from the subtropics into the North Atlantic. The subsequent chain of events involves a continuous increase in deep water formation in the Southern Ocean and a reduction in northward transport of salt and heat. The high-latitude North Atlantic gradually freshens and AABW continues to expand northwards. 24 kyr into the simulation, the AMOC has weakened to ~14.5 Sv. At this point, the AMOC strength drops abruptly by 1 Sv as the reduced salinity advection into the North Atlantic effectively constitutes a weak freshwater hosing and heat convergence, an indicator for a reduced reach of AMOC-related heat advection, is reduced off the British Isles. This results in an increased spread of AABW into the North Atlantic and diminished sinking and heat convergence. As the latitudinal salinity gradient weakens further and AABW increasingly fills the deep North Atlantic, 27 kyr into the simulation heat advection to >55 °N stops entirely and the main North Atlantic convection site shifts southwards. During this shift, the AMOC strength decreases by an additional 2.5 Sv. Arctic waters enter the polar North Atlantic along the European continent, stratifying the water column in the region and consolidating the southward shift of the downwelling region. Sea ice increasingly covers former areas of deep water formation. In the weakest circulation state, the location of the maximum AMOC streamfunction shifts southwards by approximately 10 degrees and up in the water column by 400 m initially (28.5 kyr) and eventually almost 800 m (47 kyr) This shift allows cold, less dense arctic water masses to extend further south into the North Atlantic.

https://doi.org/10.5194/cp-2023-82
Preprint. Discussion started: 17 October 2023

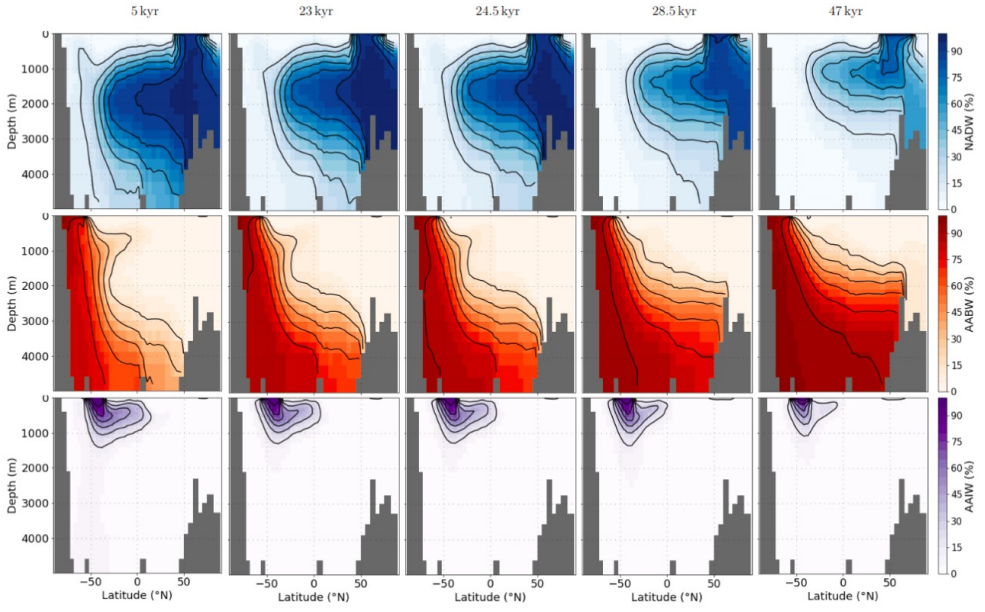

Figure 6: Atlantic water mass distributions at the five time slices of our simulation B.slow indicated in Fig. 5. Each row shows the zonally-averaged contribution of water sourced in one of three regions: the North Atlantic (upper row), the Southern Ocean (middle row), and the Southern Atlantic (bottom row), diagnosed with three passive dye tracers. Fig. SI.1 shows the spatial pattern of our dye forcing.

The changes in the AMOC streamfunction associated with the decreasing radiative forcing in experiment B.slow bear close resemblance to the changes we observed in the transient experiment set A during AMOC transitions from the interglacial to the glacial circulation state (Fig 6 and Fig SI.5 - SI.8).

We tracked the effects of these circulation changes on the distribution of intermediate and deep water masses by simulating the mixing of circulation tracers (dyes) from downwelling regions (fig SI.1). Figure 6 shows that, during the first 23 kyr of our simulation, AABW spreads further North and occupies increasingly shallower depths while the northward reach of AAIW is reduced. Accordingly, NADW shoals as it is unable to fully replace AABW in the deep North Atlantic. The reduced export of NADW also leads to a decrease in its southward extent, contracting to 40 °S. The first abrupt shift in AMOC strength at 24.5 kyr in B.slow is accompanied by a further reduction of NADW export into the deep Atlantic, before it is entirely replaced by AABW at depth below ~3.5 km in the weakest circulation state. The continued shoaling of NADW increasingly replaces AAIW at intermediate depths until the latter effectively no longer extends toward the equator (<10%).

In our simulations, the feedback initially stabilising the overturning circulation is the compensation of surface cooling by increased heat advection into the North Atlantic. As the climate cools, sea ice expands and its southern edge in the North Atlantic approaches the downwelling locations. In addition, weakened northward transport reduces heat advection

https://doi.org/10.5194/cp-2023-82
Preprint. Discussion started: 17 October 2023

and subtropical evaporation weakens the meridional salinity gradient in the North Atlantic. The downwelling zones are sensitive to heat and salt flux changes, because any reduction in sea surface temperatures (SST) increases surface density and additionally reduces evaporation in ice-free areas, thus effectively creating a small freshwater forcing and a positive feedback to the initial SST decrease. Sea ice covering the downwelling areas acts as a strong negative feedback by preventing surface ocean cooling and evaporation, stratifying the underlying water column. Sinking slows down first in the Irminger Sea while deep water formation continues in the Northeast Atlantic and south of Greenland stabilising the new circulation state. As sea ice extends into the Eastern North Atlantic, the northward reach of the AMOC is restricted and a new stable circulation state is established with increased sea ice cover >55 °N. The weakened northward transport due to the reduced AMOC leads to the influx of relatively fresh Arctic waters into the North Atlantic stabilising the water column in the entire region and producing another stable AMOC state.

The negative feedbacks stabilising the two intermediate circulation states are weaker than those that stabilise the interglacial and glacial states. In the simulations with high strongest radiative forcing, the AMOC still transitions into these intermediate circulation states but does not persist in them for long. Instead, it is immediately pushed into the next state, until it reaches the more stable glacial or interglacial state. Our stability tests demonstrate that the circulation states before and after the shifts recover from small freshwater perturbations, and thus are stable states (Fig. 5a, Fig. SI.3). In these branched off sensitivity tests, the circulation state adopted before the first AMOC threshold (at ~24 kyr), developed minor self-sustained oscillations in the order of 0.5 Sv. The next stable circulation state (~25 kyr) responds most strongly to small freshwater perturbations and is also the only circulation state in our simulation which shows increasing AMOC variability (as determined by an increase in its variance) as it approaches the next threshold (Fig. 5a, Fig. SI.4). When the forcing is reversed, the radiation increase gradually strengthens the AMOC until it rapidly transitions back into the stronger circulation state when North Atlantic sea ice has receded sufficiently for a northward shift of the convection sites. The radiative forcing at which the AMOC transitions from one circulation state to the other is not equal for decreasing and increasing radiative forcing. Following typical hysteresis behaviour, a stronger negative radiative forcing is required to push the AMOC into its weak circulation state than for the transition out of it (Fig. 4b).

Our sensitivity tests with different orbital configurations indicate that the existence of AMOC thresholds and hysteresis behaviour under radiative forcing is not dependent on the initial orbital configuration. However, the AMOC is slightly more sensitive to perturbations when initiated with the orbital configuration equivalent to 30 ka before the present. In this case, the threshold for the AMOC to transition to its weaker state is reached ~1 kyr earlier than under PI or 50 ka orbital configurations (simulations B.short.30ka, B.short.PI, Fig. SI.9). The processes that affect AMOC behaviour in simulation set B also cause AMOC changes over the transiently simulated 800 kyr in simulation set A, but the circulation states adopted vary slightly in sea ice extent, hydrological cycle and salinity distribution under varying orbital configurations.

https://doi.org/10.5194/cp-2023-82
Preprint. Discussion started: 17 October 2023

3.3. Comparison with other modelling studies and proxy data

In our transient simulations covering the past 800 kyr, the AMOC strength decreases during glacial phases solely due to changes in buoyancy, the hydrological cycle and sea ice that are induced by orbital, greenhouse gas and dust-driven temperature changes. The existence of multiple stable AMOC states under varying thermal or radiative forcings has been found in various GCMs (e.g. Oka et al., 2012, Brown and Galbraith, 2016, Klockmann et al., 2018). In agreement with previous studies, we found multiple (meta)stable AMOC circulation modes for radiative forcing levels between full glacial and interglacial climates. Moreover, we find that the transitions between these states occur abruptly, some within as little as 100 years. Similar to the observations made by Oka et al. (2021), these AMOC transitions arise from salt redistribution in the ocean and sea ice expansion into deep convection zones, though in our simulations heat advection is important too. In our simulations, each transition in AMOC strength is associated with a shift in the convergence of heat and salt fluxes and a southward expansion of sea ice into the North Atlantic which increasingly decouples the surface ocean buoyancy from the atmosphere. In the meta-stable states, the density gradients in the main North Atlantic deep convection zones are strongly dependent on surface buoyancy fluxes. In these states, small changes in buoyancy or sea ice cover can cause resumption or cessation of convection, which makes the AMOC sensitive to small perturbations. The AMOC is only pushed into its weakest state when the net heat advection into the North Atlantic has ceased and all convection sites are sea ice-covered. In their examination of thermal forcing of both hemispheres in an ocean-only model, Oka et al. (2021) found that thermal AMOC thresholds only exist in the ocean-only MIROC model if the Southern Hemisphere is cooled more than the Northern Hemisphere. In our simulations with Bern3D, we find thermal thresholds also with similar cooling rates in both hemispheres, but only after applying global cooling for about six thousand years. It could thus be that thermal thresholds were previously not identified in the higher resolution model because of shorter simulation times. Another possibility is that the AMOC in our simulations responds differently to cooling, as our simulations include effects of a thermally responsive atmosphere with a climate-driven freshwater balance. The depth-integrated meridional density gradient in the North Atlantic plays a crucial role in determining the strength of convection and hence AMOC strength (De Boer et al., 2010, Johnson et al., 2019). In our simulations, this gradient is controlled by the meridional temperature gradient, the northward transport of subtropical waters which is regulated by the AMOC, and the meteoric freshwater balance. Climate cooling reduces evaporation, the water-holding capacity of the atmosphere and the atmospheric poleward transport of moisture. Consequently, an additional positive feedback mechanism is established, whereby cooling causes freshwater balance changes and thereby alter the meridional salinity gradient which, in addition to changed ocean circulation and thermal insulation from sea ice formation, influences AMOC stability and affects the stabilities of the different circulation states.

https://doi.org/10.5194/cp-2023-82
Preprint. Discussion started: 17 October 2023

Climate of the Past Discussions
Open Access
EGU

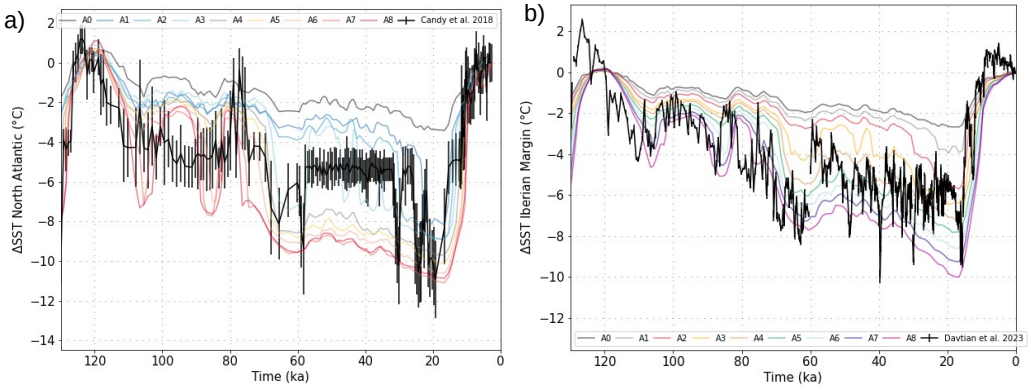

Figure 7: Simulated and reconstructed SST differences from PI over the last glacial cycle in the North Atlantic (a, reconstruction by Candy and Alonso-Garcia, 2018) and on the Iberian Margin (b, reconstruction by Davtian and Bard, 2023). The model data was interpolated to the time points for which proxy reconstructions exist.

By testing a wide range of glacial-interglacial temperature changes, our experiments demonstrate that the cooling during glacial periods could have contributed to a weakened AMOC (independent of external freshwater fluxes), but how realistic are the simulated changes? Unlike in our simulations, most GCMs participating in PMIP4 do not show a shallowing or weakening of the overturning cell under LGM boundary conditions (Sherriff-Tadano and Klockmann, 2021). The difference could arise from the static wind fields that we prescribe, since an ice-sheet related increase in wind speeds over the North Atlantic leads to a strengthened AMOC (Klockmann et al., 2018), or different representations of processes affecting AABW density changes. A shallower and likely weaker AMOC during peak glacials is however consistent with observational data (Lynch-Stieglitz et al., 2017, Pöppelmeier et al., 2023). In Fig. 7, simulated SST changes in between Ireland and the Iceland Basin and on the Iberian Margin are compared to proxy-based reconstructions. Circulation changes alter the distribution of heat in the North Atlantic, and simulated SST patterns are strongly affected by AMOC changes. In response to the stepwise AMOC weakening, simulated Atlantic SST also transitions stepwise from the interglacial to glacial maximum. Step changes are also an established feature of Atlantic SST reconstructions over the last glacial cycle (fig. 7), with the biggest steps at 120-110 ka and 80-60 ka also captured in our simulations. During glacial inception between 120 ka and 70 ka, the amplitudes of reconstructed SST changes in both locations resemble those simulated with strong radiative forcing (simulations A6, A7, A8). Afterwards, SSTs in those simulations decrease more than in the reconstructions, and the latter closer align with weaker radiative forcing (simulations A3, A4). After ~70 ka, shorter climatic events (Heinrich and Dansgaard-Oeschger) that are not part of our simulations are more frequent than before and could affect the comparability between reconstructed and simulated SST. Additionally, the further into the glacial cycle, the more the topography and wind fields would have deviated from their pre-industrial states that we keep constant throughout the simulations. These factors could cause a shift in AMOC and SST changes that are not captured by our simulations.

https://doi.org/10.5194/cp-2023-82
Preprint. Discussion started: 17 October 2023

Climate of the Past Discussions
Open Access
EGU

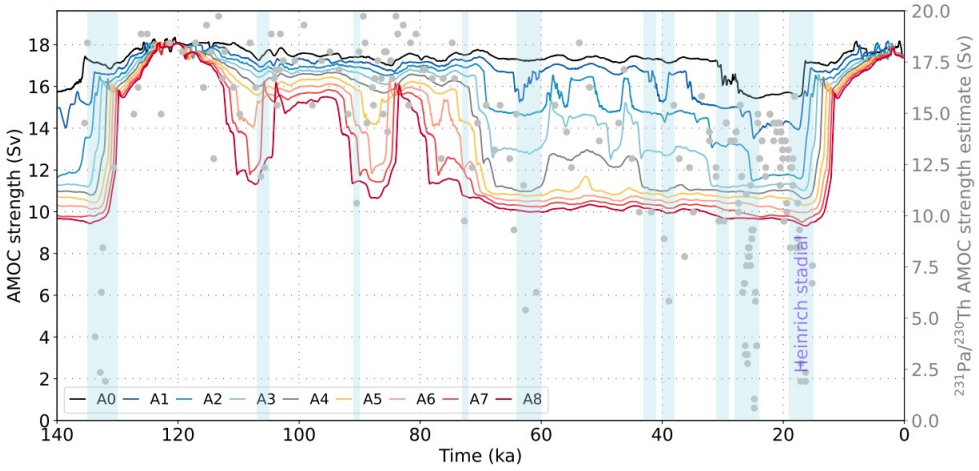

Figure 8: Simulated AMOC changes due to thermal forcing over the last 140 kyr. Gray dots indicate AMOC strength estimated from $^{231}Pa/^{230}Th$ (Böhm et al., 2015, Lippold et al., 2009) by assuming a sensitivity of -0.0024 Sv^{-1} (Rempfer et al., 2017).

Fig. 8 compares the simulated changes in AMOC strength over the last 120 kyr in simulation set A to indications of AMOC weakening based on $^{231}Pa/^{230}Th$ from the Bermuda Rise (Böhm et al., 2015). These simulations A2-A4 have a PI-LGM GMST differences of 4.7-6.2°C (within the proxy-constrained and PMIP range and close to the most recent estimate of 6.1°C by Tierney et al., 2020) and show a shift to a weaker AMOC at the beginning of MIS 4 around 70 ka ago, when a negative $^{231}Pa/^{230}Th$ shift occurred. While the simulated radiation-driven AMOC changes cannot explain weaker or collapsed circulation states (<11 Sv) during Heinrich stadials, this comparison shows that the long term AMOC weakening during glacial phases could have been driven by temperature changes. It is important to note that AMOC strength estimates based on this $^{231}Pa/^{230}Th$ record need to be treated with caution. Pöppelmeier et al. (2021; 2023) showed a strong local influence on sedimentary proxies at this site, and we did not correct the $^{231}Pa/^{230}Th$ signal for potential productivity changes.

3.4. Meta-stable AMOC modes

Finally, we can test whether the simulated changes of AMOC variability over glacial cycles are realistic. Using our 800 kyr long simulations, we determine how often and when radiative forcing pushed the AMOC into circulation states with high AMOC variability under each forcing (Fig. 9). In all simulations with dust forcing, the AMOC transitions into excitable states in all of the past eight glacial cycles, but the timing of these shifts varies. For example, during the ultimate glacial cycle, the simulations A2-A4 exhibit an intermediate circulation mode during MIS 3 which is also characterised by an increased frequency of AMOC mode shifts (see fig. 3). Similar rapid mode switches occur earlier in the glacial cycle, i.e. during MIS 5d-e in simulations A6-A8. In these simulations, the AMOC already transitions into the glacial circulation state at the beginning of MIS 4. In simulations A1-A3, the AMOC persists in these states for several tens of thousands of years at a time, during most glacials. Under stronger radiative forcing, the periods in which AMOC adopts these states are shorter and mostly occur at the start of glacial cycles.

https://doi.org/10.5194/cp-2023-82
Preprint. Discussion started: 17 October 2023

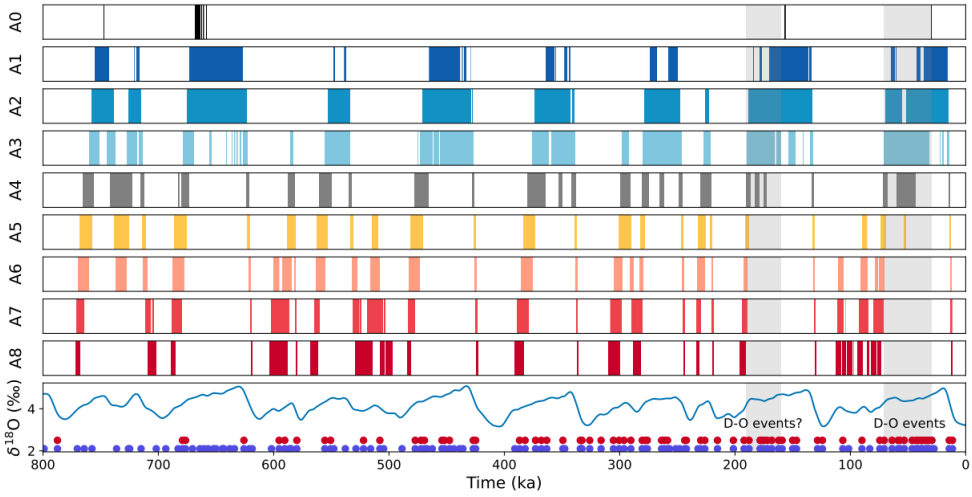

Figure 9: Occurrence of the more excitable intermediate AMOC states due to radiative forcing over the last 800 kyr in simulation set A. The time periods with intermediate AMOC states are marked as vertical bars, each row showing the results for a different forcing magnitude from simulation set A. At the bottom, $\delta^{18}O$ from Lisiecki and Raymo (2005) is shown for reference, alongside the time period with confirmed and suspected Dansgaard-Oeschger events (light gray bars based on Rousseau et al., 2020, blue and red circles are based on reconstructions Barker et al., 2011, who used two different detection thresholds).

We can assess the skill of our simulations at predicting meta-stable AMOC states from the radiative forcing by comparing the output with records of high AMOC variability in the past. Simulations A3 and A4 shift into a meta-stable circulation state during MIS 3, and similarly between 190 and 160 ka during the penultimate glacial cycle, and prior to each previous glacial maximum but not during the glacial maxima themselves. A meta-stable AMOC state during these intervals seems realistic given the high frequency of Dansgaard-Oeschger events in MIS 3 and the suspected occurrence of Dansgaard-Oeschger events during MIS 6 (Rousseau et al. 2020). Similarly, Barker et al. (2011), who predicted the occurrence of Dansgaard-Oeschger events during previous glacial cycles based on the Antarctic temperature record (with two different identification thresholds, red and blue circles in Fig. 9) following the approach of Siddall et al. (2006), found a high frequency of occurrence of Dansgaard-Oeschger events during MIS 3 and 6, but also throughout most glacial phases. None of our simulations predicts such a ubiquity of meta-stable AMOC states, possibly due to the prescribed boundary conditions although the detection method of Barker et al. (2011) is also more uncertain for glacial cycles further back in time. The consistency of the simulated radiation-induced AMOC instability with observational indication of millennial-scale AMOC variability at least during MIS 3 and 6 in simulations A3 and A4 suggests that these could present a more realistic temporal AMOC evolution than the others. Simulations A3 and A4 also exhibit PI-LGM temperature differences of 5.4 and 6.2°C, respectively, close to the proxy-constrained reconstruction (Tierney et al., 2020), and roughly reproduce the reconstructed regional SST changes and reduced circulation strength in MIS 3 and 2 (Fig. 7 and 8).

https://doi.org/10.5194/cp-2023-82
Preprint. Discussion started: 17 October 2023

Thermal conditioning of AMOC excitability is in line with studies that found the existence of a 'sweet spot' in atmospheric CO_2 radiative forcing which is particularly conducive to short, abrupt AMOC perturbations and/or self-sustained AMOC oscillations (e.g. Li and Born, 2019, Vettoretti et al., 2022). Yet, our simulations do not produce such perturbations, partly due to the smoothed forcing and static wind fields (see discussion of model limitations below). The transient circulation state switches in response to orbitally-paced radiation changes in our simulations are much weaker than those found in other studies (Vettoretti et al., 2022, Klockmann et al., 2018, Kuniyoshi et al., 2022), and our simulations do not contain oscillations that could directly be compared to Dansgaard-Oeschger events.

3.5. Model limitations

There are limitations to our study, such that we would not expect a close model-data match with the paleo-record given that our simulations lack some but important glacial boundary conditions and forcings. The location of deep convection is dependent on wind fields, bathymetry, and grid resolution, and thus the AMOC thresholds are model and forcing dependent. The forcing applied in our simulations captures the albedo effect of varying terrestrial ice sheet extent, but we do not consider their orography or sea level effects, including impacts on the atmospheric circulation. Previous studies suggested that pre-industrial or intermediate ice sheet configurations are required to produce a thermal AMOC threshold in the range of glacial-interglacial CO_2 concentrations and that the presence of a full glacial Laurentide ice sheet prevents such a threshold (e.g. Klockmann et al., 2018, Malmierca-Vallet and Sime, 2022). Yet Oka et al. (2012) argue that the LGM thermal threshold value is likely very sensitive to model design and forcings. Further investigations are needed to determine how changes in strength and location of the wind stress due to the ice sheet's orography would affect sea ice formation in the northern North Atlantic and the AMOC thresholds in our simulations (Li and Born, 2019).

4. Conclusions

Our study demonstrates the existence of thermal AMOC thresholds and multiple stable circulation states in the Bern3D model. This adds to previous studies showing that thermal AMOC thresholds emerge in a range of Earth system models varying in complexity and number of components coupled (Zhang et al., 1993), in particular, they also arise in an energetically and hydrologically coupled ocean-sea ice-atmosphere model of intermediate complexity like Bern3D. These thresholds shape the response in the simulated AMOC to radiative orbital and atmospheric composition-driven temperature changes over the last 800 kyr. During this period the AMOC transitions between up to four stable circulation states. The full glacial and interglacial circulation states are most stable, as relatively strong forcing is required to push the AMOC out of them. In contrast, the intermediate AMOC states are more sensitive to perturbations as small variations in orbital and radiative forcing are able to push the circulation out of these states. This behaviour resembles the one found in more complex General Circulation Models that exhibit self-sustained oscillations at 'sweetspot' CO_2 levels, which lie between glacial and interglacial values. Thus, our simulations suggest that radiative forcing could have created highly sensitive intermediate AMOC states repeatedly over the last 800 kyr.

Data availability

https://doi.org/10.5194/cp-2023-82
Preprint. Discussion started: 17 October 2023

All simulation output necessary to produce the figures in this manuscript are available at https://doi.org/10.5281/zenodo.8424878
Proxy data plotted against the simulation output for comparison was taken from public repositories and are available via the citations provided.

Author contributions

AJT ran the simulations. MA analysed the output and drafted the manuscript. All authors contributed to the interpretation of the results and the final manuscript text.

Conflicts of interest

The authors declare that they have no conflict of interest.

Acknowledgements

MA, AJT and FJ were financially supported by the Swiss National Science Foundation (#200020_200511).

FP was financially supported by the European Union's Horizon 2020 research and innovation programme under grant agreements no. 101023443 (project CliMoTran).

TFS and FP were financially supported by the European Union's Horizon 2020 research and innovation programme under grant agreements no. 820970 (project TiPES), and the Swiss National Science Foundation's project 200020_200492.

Calculations were performed on UBELIX (http://www.id.unibe.ch/hpc), the HPC cluster at the University of Bern.

References

Albani, S., Balkanski, Y., Mahowald, N., Winckler, G., Maggi, V. and Delmonte, B., 2018. Aerosol-climate interactions during the Last Glacial Maximum. *Current Climate Change Reports*, *4*, pp.99-114.

Armstrong, E., Izumi, K. and Valdes, P., 2022. Identifying the mechanisms of DO-scale oscillations in a GCM: a salt oscillator triggered by the Laurentide ice sheet. Climate Dynamics, pp.1-19.

Bard, E., Arnold, M., Maurice, P., Duprat, J., Moyes, J. and Duplessy, J.C., 1987. Retreat velocity of the North Atlantic polar front during the last deglaciation determined by 14C accelerator mass spectrometry. *Nature*, *328*(6133), pp.791-794.

Barker, S., Knorr, G., Edwards, R.L., Parrenin, F., Putnam, A.E., Skinner, L.C., Wolff, E. and Ziegler, M., 2011. 800,000 years of abrupt climate variability. *science*, *334*(6054), pp.347-351.

https://doi.org/10.5194/cp-2023-82
Preprint. Discussion started: 17 October 2023

Bereiter, B., Eggleston, S., Schmitt, J., Nehrbass-Ahles, C., Stocker, T.F., Fischer, H., Kipfstuhl, S. and Chappellaz, J., 2015. Revision of the EPICA Dome C CO2 record from 800 to 600 kyr before present. *Geophysical Research Letters*, *42*(2), pp.542-549.

Berger, A., 1978. Long-term variations of caloric insolation resulting from the Earth's orbital elements. *Quaternary research*, *9*(2), pp.139-167.

Berger, A. and Loutre, M.F., 1991. Insolation values for the climate of the last 10 million years. *Quaternary science reviews*, *10*(4), pp.297-317.

Böhm, E., Lippold, J., Gutjahr, M., Frank, M., Blaser, P., Antz, B., Fohlmeister, J., Frank, N., Andersen, M.B. and Deininger, M., 2015. Strong and deep Atlantic meridional overturning circulation during the last glacial cycle. *Nature*, *517*(7532), pp.73-76.

Bozbiyik, A., Steinacher, M., Joos, F., Stocker, T.F. and Menviel, L., 2011. Fingerprints of changes in the terrestrial carbon cycle in response to large reorganizations in ocean circulation. Climate of the Past, 7(1), pp.319-338.

Broecker, W.S., 1994. Massive iceberg discharges as triggers for global climate change. *Nature*, *372*(6505), pp.421-424.

Brown, N. and Galbraith, E.D., 2016. Hosed vs. unhosed: interruptions of the Atlantic Meridional Overturning Circulation in a global coupled model, with and without freshwater forcing. Climate of the Past, 12(8), pp.1663-1679.

Candy, I. and Alonso-Garcia, M., 2018. A 1 Ma sea surface temperature record from the North Atlantic and its implications for the early human occupation of Britain. *Quaternary Research*, *90*(2), pp.406-417.

Dansgaard, W., Johnsen, S.J., Clausen, H.B., Dahl-Jensen, D., Gundestrup, N.S., Hammer, C.U., Hvidberg, C.S., Steffensen, J.P., Sveinbjörnsdottir, A.E., Jouzel, J. and Bond, G., 1993. Evidence for general instability of past climate from a 250-kyr ice-core record. *nature*, *364*(6434), pp.218-220.

Davtian, N. and Bard, E., 2023. A new view on abrupt climate changes and the bipolar seesaw based on paleotemperatures from Iberian Margin sediments. *Proceedings of the National Academy of Sciences*, *120*(12), p.e2209558120.

De Boer, A.M., Gnanadesikan, A., Edwards, N.R. and Watson, A.J., 2010. Meridional density gradients do not control the Atlantic overturning circulation. *Journal of Physical Oceanography*, *40*(2), pp.368-380.

Edwards, N. R., Willmott, A. J., and Killworth, P. D.: On the role of topography and wind stress on the stability of the thermohaline circulation, J. Phys. Oceanogr., 28, 756–778, https://doi.org/10.1175/1520-0485(1998)028<0756:OTROTA>2.0.CO;2, 1998.

Fischer, H., Meissner, K.J., Mix, A.C., Abram, N.J., Austermann, J., Brovkin, V., Capron, E., Colombaroli, D., Daniau, A.L., Dyez, K.A. and Felis, T., 2018. Palaeoclimate constraints on the impact of 2 C anthropogenic warming and beyond. *Nature geoscience*, *11*(7), pp.474-485.

Griffies, S. M.: The Gent–McWilliams Skew Flux, J. Phys. Oceanogr., 28, 831–841, https://doi.org/10.1175/1520-0485(1998)028<0831:TGMSF>2.0.CO;2, 1998.

https://doi.org/10.5194/cp-2023-82
Preprint. Discussion started: 17 October 2023

Grousset, F.E., Pujol, C., Labeyrie, L., Auffret, G. and Boelaert, A., 2000. Were the North Atlantic Heinrich events triggered by the behavior of the European ice sheets?. *Geology*, *28*(2), pp.123-126.

Haskins, R.K., Oliver, K.I., Jackson, L.C., Wood, R.A. and Drijfhout, S.S., 2020. Temperature domination of AMOC weakening due to freshwater hosing in two GCMs. Climate Dynamics, 54, pp.273-286.

Heinrich, H., 1988. Origin and consequences of cyclic ice rafting in the northeast Atlantic Ocean during the past 130,000 years. *Quaternary research*, *29*(2), pp.142-152.

Ivanovic, R.F., Valdes, P.J., Gregoire, L., Flecker, R. and Gutjahr, M., 2014. Sensitivity of modern climate to the presence, strength and salinity of Mediterranean-Atlantic exchange in a global general circulation model. Climate dynamics, 42, pp.859-877.

Jackson, L.C., Schaller, N., Smith, R.S., Palmer, M.D. and Vellinga, M., 2014. Response of the Atlantic meridional overturning circulation to a reversal of greenhouse gas increases. Climate dynamics, 42, pp.3323-3336.

Jackson, L.C. and Wood, R.A., 2018. Hysteresis and resilience of the AMOC in an eddy-permitting GCM. *Geophysical Research Letters*, *45*(16), pp.8547-8556.

Jackson, L.C., Alastrué de Asenjo, E., Bellomo, K., Danabasoglu, G., Haak, H., Hu, A., Jungclaus, J.H., Lee, W., Meccia, V.L., Saenko, O. and Shao, A., 2023. Understanding AMOC stability: the North Atlantic hosing model intercomparison project. Geoscientific Model Development, 16, pp.1975-1995.

Johnson, H.L., Cessi, P., Marshall, D.P., Schloesser, F. and Spall, M.A., 2019. Recent contributions of theory to our understanding of the Atlantic meridional overturning circulation. *Journal of Geophysical Research: Oceans*, *124*(8), pp.5376-5399.

Joos, F. and Spahni, R., 2008. Rates of change in natural and anthropogenic radiative forcing over the past 20,000 years. *Proceedings of the National Academy of Sciences*, *105*(5), pp.1425-1430.

Joos, H., Madonna, E., Witlox, K., Ferrachat, S., Wernli, H. and Lohmann, U., 2017. Effect of anthropogenic aerosol emissions on precipitation in warm conveyor belts in the western North Pacific in winter–a model study with ECHAM6-HAM. Atmospheric chemistry and physics, 17(10), pp.6243-6255.

Kageyama, M., Harrison, S.P., Kapsch, M.L., Lofverstrom, M., Lora, J.M., Mikolajewicz, U., Sherriff-Tadano, S., Vadsaria, T., Abe-Ouchi, A., Bouttes, N. and Chandan, D., 2021. The PMIP4 Last Glacial Maximum experiments: preliminary results and comparison with the PMIP3 simulations. *Climate of the Past*, *17*(3), pp.1065-1089.

Klockmann, M., Mikolajewicz, U. and Marotzke, J., 2018. Two AMOC states in response to decreasing greenhouse gas concentrations in the coupled climate model MPI-ESM. Journal of Climate, 31(19), pp.7969-7984.

Klockmann, M., Mikolajewicz, U., Kleppin, H. and Marotzke, J., 2020. Coupling of the subpolar gyre and the overturning circulation during abrupt glacial climate transitions. Geophysical Research Letters, 47(21), p.e2020GL090361.

Kuniyoshi, Y., Abe-Ouchi, A., Sherriff-Tadano, S., Chan, W.L. and Saito, F., 2022. Effect of Climatic Precession on Dansgaard-Oeschger-Like Oscillations. *Geophysical Research Letters*, *49*(6), p.e2021GL095695.

https://doi.org/10.5194/cp-2023-82
Preprint. Discussion started: 17 October 2023

Li, C. and Born, A., 2019. Coupled atmosphere-ice-ocean dynamics in Dansgaard-Oeschger events. Quaternary Science Reviews, 203, pp.1-20.

Lippold, J., Grützner, J., Winter, D., Lahaye, Y., Mangini, A. and Christl, M., 2009. Does sedimentary 231Pa/230Th from the Bermuda Rise monitor past Atlantic meridional overturning circulation?. *Geophysical Research Letters*, *36*(12).

Lisiecki, L. E. & Raymo, M. E. A, 2005. Pliocene-Pleistocene stack of 57 globally distributed benthic d18O records. Paleoceanography 20, PA1003, doi:10.1029/ 2004PA001071.

Lisiecki, L.E. and Stern, J.V., 2016. Regional and global benthic δ18O stacks for the last glacial cycle. *Paleoceanography*, *31*(10), pp.1368-1394.

Liu, W., Xie, S.P., Liu, Z. and Zhu, J., 2017. Overlooked possibility of a collapsed Atlantic Meridional Overturning Circulation in warming climate. *Science Advances*, *3*(1), p.e1601666.

Loulergue, L., Schilt, A., Spahni, R., Masson-Delmotte, V., Blunier, T., Lemieux, B., Barnola, J.M., Raynaud, D., Stocker, T.F. and Chappellaz, J., 2008. Orbital and millennial-scale features of atmospheric CH4 over the past 800,000 years. *Nature*, *453*(7193), pp.383-386.

Lynch-Stieglitz, J., 2017. The Atlantic meridional overturning circulation and abrupt climate change. *Annual review of marine science*, *9*, pp.83-104.

Malmierca-Vallet, Irene, Louise C. Sime and the D-O community members. "Dansgaard-Oeschger events in climate models: Review and baseline MIS3 protocol." *Climate of the Past*, *19*(5), pp.915-942.

Masson-Delmotte, V., Schulz, M., Abe-Ouchi, A., Beer, J., Ganopolski, A., González Rouco, J.F., Jansen, E., Lambeck, K., Luterbacher, J., Naish, T. and Osborn, T., 2013. Information from paleoclimate archives. In IPCC AR5 Climate Change 2013 - The Physical Science Basis (eds Stocker, T. et al.), *383464*, p.2013.

Menviel, L., Joos, F. and Ritz, S.P., 2012. Simulating atmospheric CO2, 13C and the marine carbon cycle during the Last Glacial–Interglacial cycle: possible role for a deepening of the mean remineralization depth and an increase in the oceanic nutrient inventory. Quaternary Science Reviews, 56, pp.46-68.

Oka, A., Hasumi, H. and Abe-Ouchi, A., 2012. The thermal threshold of the Atlantic meridional overturning circulation and its control by wind stress forcing during glacial climate. Geophysical Research Letters, 39(9).

Oka, A., Abe-Ouchi, A., Sherriff-Tadano, S., Yokoyama, Y., Kawamura, K. and Hasumi, H., 2021. Glacial mode shift of the Atlantic meridional overturning circulation by warming over the Southern Ocean. Communications Earth & Environment, 2(1), p.169.

Okazaki, Y., Timmermann, A., Menviel, L., Harada, N., Abe-Ouchi, A., Chikamoto, M.O., Mouchet, A. and Asahi, H., 2010. Deepwater formation in the North Pacific during the last glacial termination. Science, 329(5988), pp.200-204.

Pedro, J.B., Jochum, M., Buizert, C., He, F., Barker, S. and Rasmussen, S.O., 2018. Beyond the bipolar seesaw: Toward a process understanding of interhemispheric coupling. Quaternary Science Reviews, 192, pp.27-46.

https://doi.org/10.5194/cp-2023-82
Preprint. Discussion started: 17 October 2023

Pöppelmeier, F., Scheen, J., Jeltsch-Thömmes, A. and Stocker, T.F., 2020. Simulated stability of the AMOC during the Last Glacial Maximum under realistic boundary conditions. *Climate of the Past*, *2021 17, no. 2 (2021): 615-632.*

Pöppelmeier, F., Jeltsch-Thömmes, A., Lippold, J., Joos, F. and Stocker, T.F., 2023. Multi-proxy constraints on Atlantic circulation dynamics since the last ice age. *Nature geoscience*, *16*(4), pp.349-356.

Praetorius, S.K. and Mix, A.C., 2014. Synchronization of North Pacific and Greenland climates preceded abrupt deglacial warming. Science, 345(6195), pp.444-448.

Rahmstorf, S., 1996. On the freshwater forcing and transport of the Atlantic thermohaline circulation, Clim. Dyn., 12, 799–811.

Rahmstorf, S., 1998. Influence of Mediterranean outflow on climate. Eos, Transactions American Geophysical Union, 79(24), pp.281-282.

Rempfer, J., Stocker, T.F., Joos, F., Lippold, J. and Jaccard, S.L., 2017. New insights into cycling of 231Pa and 230Th in the Atlantic Ocean. *Earth and Planetary Science Letters*, *468*, pp.27-37.

Rousseau, D.D., Antoine, P., Boers, N., Lagroix, F., Ghil, M., Lomax, J., Fuchs, M., Debret, M., Hatté, C., Moine, O. and Gauthier, C., 2020. Dansgaard–Oeschger-like events of the penultimate climate cycle: the loess point of view. *Climate of the Past*, *16*(2), pp.713-727.

Ruddiman, W.F. and McIntyre, A., 1981. The North Atlantic Ocean during the last deglaciation. *Palaeogeography, Palaeoclimatology, Palaeoecology*, *35*, pp.145-214.

Severinghaus, J.P., Beaudette, R., Headly, M.A., Taylor, K. and Brook, E.J., 2009. Oxygen-18 of O2 records the impact of abrupt climate change on the terrestrial biosphere. Science, 324(5933), pp.1431-1434.

Sherriff-Tadano, S. and Klockmann, M., 2021. PmiP contributions to understanding the deep ocean circulation of the last glacial maximum. *Past Global Changes Magazine*, *29*(2), pp.84-85.

Siddall, M., T.F. Stocker, T. Blunier, R. Spahni, J. McManus, and E. Bard, Using a maximum simplicity paleoclimate model to simulate millennial variability during the last four glacial periods, Quat. Sci. Rev., 25, 3185-3197, 2006.

Stocker, T.F., and D.G. Wright, Rapid transitions of the ocean's deep circulation induced by changes in surface water fluxes, Nature, 351, 729-732, 1991.

Stocker, T.F., 2000. Past and future reorganizations in the climate system. Quaternary Science Reviews, 19(1-5), pp.301-319.

Stommel, H., 1961. Thermohaline convection with two stable regimes of flow. Tellus, 13(2), 224– 230. https://doi.org/10.3402/tellusb.v13i2.12985

Swingedouw, D., Colin, C., Eynaud, F., Ayache, M. and Zaragosi, S., 2019. Impact of freshwater release in the Mediterranean Sea on the North Atlantic climate. Climate Dynamics, 53, pp.3893-3915.

https://doi.org/10.5194/cp-2023-82
Preprint. Discussion started: 17 October 2023

Swingedouw, D., Houssais, M.N., Herbaut, C., Blaizot, A.C., Devilliers, M. and Deshayes, J., 2022. AMOC Recent and Future Trends: A Crucial Role for Oceanic Resolution and Greenland Melting?. *Frontiers in Climate*, p.32.

Tetard, M., Licari, L. and Beaufort, L., 2017. Oxygen history off Baja California over the last 80 kyr: A new foraminiferal-based record. Paleoceanography, 32(3), pp.246-264.

Tierney, J.E., Zhu, J., King, J., Malevich, S.B., Hakim, G.J. and Poulsen, C.J., 2020. Glacial cooling and climate sensitivity revisited. *Nature*, *584*(7822), pp.569-573.

Timmermann, A. and Friedrich, T., 2016. Late Pleistocene climate drivers of early human migration. Nature, 538(7623), pp.92-95.

Vettoretti, G., Ditlevsen, P., Jochum, M. and Rasmussen, S.O., 2022. Atmospheric CO2 control of spontaneous millennial-scale ice age climate oscillations. Nature Geoscience, 15(4), pp.300-306.

Wang, Y.J., Cheng, H., Edwards, R.L., An, Z.S., Wu, J.Y., Shen, C.C. and Dorale, J.A., 2001. A high-resolution absolute-dated late Pleistocene monsoon record from Hulu Cave, China. Science, 294(5550), pp.2345-2348.

Weijer, W., Cheng, W., Drijfhout, S.S., Fedorov, A.V., Hu, A., Jackson, L.C., Liu, W., McDonagh, E.L., Mecking, J.V. and Zhang, J., 2019. Stability of the Atlantic Meridional Overturning Circulation: A review and synthesis. *Journal of Geophysical Research: Oceans*, *124*(8), pp.5336-5375.

Zhang, S., Greatbatch, R.J. and Lin, C.A., 1993. A reexamination of the polar halocline catastrophe and implications for coupled ocean-atmosphere modeling. Journal of Physical Oceanography, 23(2), pp.287-299.